

Why Do Baroclinic Waves Tilt Poleward with Height?*

JEFFREY H. YIN AND DAVID S. BATTISTI

Department of Atmospheric Sciences, University of Washington, Seattle, Washington

(Manuscript received 27 November 2002, in final form 20 January 2004)

ABSTRACT

Theoretical and modeling studies of nongeostrophic effects in baroclinic waves predict that baroclinic waves should tilt poleward with height, with a larger tilt in total meridional wind than in geostrophic quantities. Regression analysis of NCEP–NCAR reanalysis 6-hourly data demonstrates that observed baroclinic waves do indeed tilt poleward with height, although the observed tilt is smaller than predicted by previous studies. The meridional ageostrophic wind enhances the poleward tilt of meridional wind perturbations, despite being smaller in amplitude than the meridional geostrophic wind by a factor of 5.

An improved estimate of the structure of the meridional ageostrophic wind in baroclinic waves is calculated assuming force balance. Several important terms in this estimate have been left out of previous estimates of the meridional ageostrophic wind. Three terms in the improved estimate produce nearly all of the poleward tilt of the meridional wind: 1) the advection of geostrophic zonal wind perturbations by the mean zonal wind, 2) the convergence of the eddy momentum flux, and 3) the effect of friction.

The poleward tilt with height of baroclinic waves explains why upper-level storm tracks tend to occur poleward of near-surface baroclinic regions, and may play a role in the midwinter suppression of the Pacific storm track.

1. Introduction

Most previous studies of the observed structure of baroclinic waves have focused on their structure in the longitude–latitude plane (e.g., Blackmon et al. 1984) or the longitude–height plane (e.g., Lim and Wallace 1991; Chang 1993). It is well-known that baroclinic waves tilt westward with height. However, the poleward tilt with height of baroclinic waves is less well-known, and, to our knowledge, there are no published studies of the poleward tilt of *observed* baroclinic waves. While the regression analysis of Chang (2001) suggests that meridional wind perturbations (v') in baroclinic waves simulated by a GCM tilt poleward with height by approximately 10° latitude between 850 and 250 mb, no mention of this feature was made in the paper.

The first explanations of the poleward tilt with height of baroclinic waves come from early studies of nongeostrophic effects in the Eady (1949) baroclinic stability problem. McIntyre (1965) examines the solution to the Eady problem with v' vanishing on the side boundaries. He finds that the Eady problem is separable to two orders in the Rossby number Ro beyond the

quasigeostrophic (QG) approximation if the side boundaries tilt poleward with height with a slope of $2Ro/LH$, where L and H are appropriate horizontal and vertical length scales. The same poleward tilt of v' is found by Derome and Dolph (1970) in calculations to $O(Ro)$ beyond QG theory with vertical side boundaries, as long as the boundaries are far enough away from the axis of the wave not to limit its poleward tilt. Hoskins (1975) uses the semigeostrophic (SG) equations to show that perturbations of geopotential height (z') and geostrophic velocities in Eady baroclinic waves should tilt poleward with height with a slope that is parallel to the absolute vorticity vector, while total (geostrophic plus ageostrophic) v' should have twice this slope. The slope of the absolute vorticity vector is approximately equal to the vertical shear of the mean zonal wind $\partial\bar{u}/\partial z$ divided by the Coriolis parameter f , or $U/Hf = Ro/LH$, where U is an appropriate velocity scale, so the slope of v' is again $2Ro/LH$. Hoskins (1975) uses $U \approx 30 \text{ m s}^{-1}$, $H \approx 10 \text{ km}$, and $f \approx 10^{-4} \text{ s}^{-1}$ to calculate the slope of the absolute vorticity vector as $U/Hf \approx 30$. This suggests that z' should tilt poleward by about 300 km, or 3° latitude, from the surface to the tropopause, and v' should tilt poleward by about 6° latitude.

Snyder et al. (1991) compare simulations of baroclinic waves in SG and primitive equation (PE) channel models and find that the poleward tilt with height of z' in the most unstable mode of the SG model ($\sim 300 \text{ km}$ from the surface to 9-km altitude) is smaller than that of the PE model ($\sim 500 \text{ km}$). Their examination of the

* Joint Institute for the Study of the Atmosphere and Ocean Contribution Number 962.

Corresponding author address: Jeffrey Yin, Climate and Global Dynamics Division, NCAR, P.O. Box 3000, Boulder, CO 80307-3000.
E-mail: jyin@ucar.edu

SG and PE vorticity equations reveals that the neglect of the geostrophic advection of ageostrophic vorticity in the SG model leads to an underestimation of perturbation growth on the poleward side of the jet at upper levels, and thus to an underestimation of the poleward tilt with height of z' in SG baroclinic waves. The SG and PE simulations, taken together, suggest that the vertical shear of the jet and the advection of ageostrophic vorticity contribute approximately equally to the poleward tilt with height of baroclinic waves. Assuming that the poleward tilt of v' is twice that of z' in PE baroclinic waves as well, the poleward tilt of z' in the PE simulations of Snyder et al. (1991) is approximately consistent with the poleward tilt of v' in the GCM simulations of Chang (2001).

The present study examines the poleward tilt with height of v' in observed baroclinic waves, and the structure of the ageostrophic wind that contributes to this poleward tilt. We are particularly interested in the structure of v' because advection by v' across strong meridional gradients of temperature and potential vorticity drives the growth and propagation of baroclinic waves. Section 2 provides a brief overview of the National Centers for Environmental Prediction–National Center for Atmospheric Research (NCEP–NCAR) reanalysis data and the regression analysis used in this study. Section 3 demonstrates that the ageostrophic wind is important for the poleward tilt with height of v' in observed baroclinic waves. Section 4 reviews and expands upon the work of Lim et al. (1991) and Kwon and Lim (1999) to estimate the structure of the ageostrophic wind field in baroclinic waves. Section 5 discusses the terms in the estimate of the ageostrophic wind that contribute to the poleward tilt of v' . Conclusions follow in section 6.

2. Data and analysis techniques

The data used in this study are the NCEP–NCAR reanalysis 6-hourly data from July 1979 to June 2003, which were obtained from the National Oceanic and Atmospheric Administration/Cooperative Institute for Research in Environmental Sciences (NOAA/CIRES) Climate Diagnostics Center Website (<http://www.cdc.noaa.gov>). Nearly identical results are obtained using the full NCEP–NCAR reanalysis dataset from 1948 to 2003, but we choose to use only the data from 1979 onward because the incorporation of satellite data since 1979 has improved the quality of the reanalysis. In order to perform the same analysis on each month, we divide the 360-day “year” (beginning 3 September and ending 28 August) into twelve 30-day periods that approximately correspond to calendar months (i.e., November is 2 November–1 December, January is 1 January–30 January, April is 1 April–30 April, and July is 30 June–29 July). Regressions are calculated separately for each 30-day “month,” using essentially the technique of Lim and Wallace (1991): the regression coefficient $b(i)$ for

a particular variable at a particular pressure level, latitude, and longitude is calculated as

$$b(i) = \frac{\sum_{t=1}^N y'_t(i)x'_t}{\left(\sum_{t=1}^N x'^2_t\right)^{1/2}}, \quad (1)$$

where $y_t(i)$ is the time series of the variable at the specified pressure level, latitude, and longitude; x_t is the reference time series; primes denote departures from 30-day period means; and N is the total number of 6-h periods available for the 30-day month. As explained by Chang (1993), temporal filtering can produce “ringing” in the time domain and obscure the downstream development of baroclinic waves, so we use unfiltered data for both the reference time series and the time series of the variables regressed on the reference time series.

We choose v' at 925 mb at various points in the storm tracks as our reference time series x'_t , since we have found that regressions on 925-mb v' effectively capture developing baroclinic waves; however, the poleward tilt with height is also observed in regressions on 250-mb v' . Regressions based on 925-mb v' were calculated in the regions of strongest baroclinic growth in the Pacific (37.5°N, 155°E) and Atlantic (42.5°N, 55°W) storm tracks for November, January, and April, and in the Southern Hemisphere (SH) storm track (45°S, 45°E) for July. For brevity, we show figures only for baroclinic waves over the Atlantic in January, which we argue are representative of “typical” baroclinic waves. The poleward tilt of baroclinic waves is largest over the Atlantic in January, so it is easier to illustrate the poleward tilt in January than in November or April, and the tilt is similar to that seen in the SH in July. The baroclinic waves over the Pacific have an even stronger poleward tilt, probably due to the strong Pacific jet, and have a distorted structure relative to those in the Atlantic and SH, particularly in January when the Pacific subtropical jet is strongest. In general, observations show that the poleward tilt of baroclinic waves is larger when the jet is stronger but has a smaller poleward tilt, suggesting that the poleward tilt of baroclinic waves is more related to jet strength than to the poleward tilt of the jet. We also find that, although their relative magnitudes vary, the same three terms produce most of the poleward tilt of v' in baroclinic waves in all storm tracks and months that we have investigated. We leave analysis of the variations of baroclinic wave structure from month to month and from storm track to storm track to future work.

3. Observed meridional wind structure in baroclinic waves

The importance of the ageostrophic wind in the poleward tilt of baroclinic waves is illustrated in Fig. 1, which shows total v' , geostrophic $v'(v'_g)$, and ageostro-

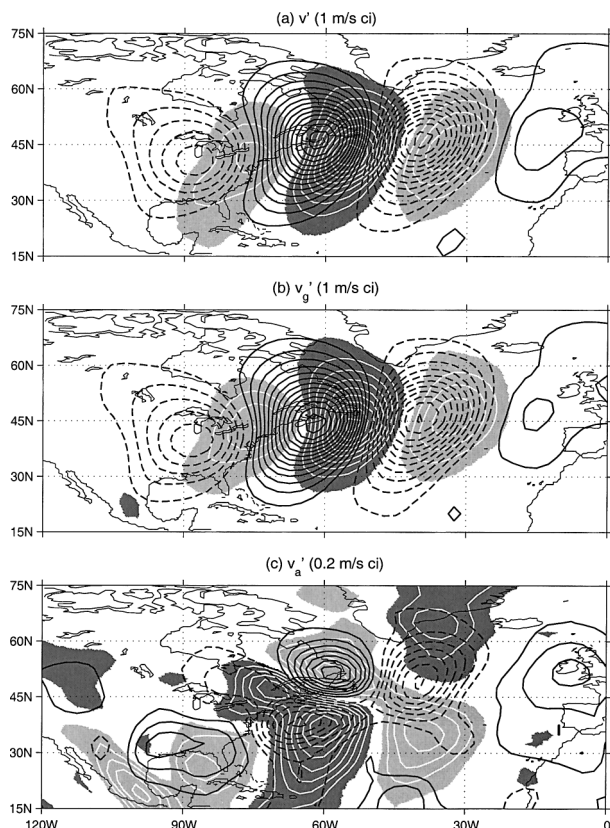


FIG. 1. Regressions of (a) total meridional wind v' , (b) geostrophic meridional wind v'_g , and (c) ageostrophic meridional wind v'_a on 925-mb v' at 42.5°N , 55°W . Black contours show values at 250 mb, with negative contours dashed and the zero contour omitted. Shading with white contours shows values at 925 mb, with light shading indicating negative values and dark shading positive values; there is no shading within one contour interval of zero. The contour interval is 1 m s^{-1} in (a) and (b), and 0.2 m s^{-1} in (c).

phic $v'(v'_a)$ at 250 mb (black contours) and 925 mb (shaded with white contours). The westward tilt with height is apparent for both v' and v'_g . However, focusing on the poleward tilt of the positive v' center located near 55°W at 925 mb and near 61°W at 250 mb, it is clear that the poleward tilt of v' is due to the ageostrophic contribution to v' ; the poleward tilt is $\sim 4^\circ$ latitude for v' and not more than 1° latitude for v'_g , which has approximately the same tilt as z' (not shown). The 250-mb zonal wind in this region is $\sim 30 \text{ m s}^{-1}$, so Hoskins (1975) predicts that v'_g should tilt by $\sim 3^\circ$ latitude from the surface to 250 mb, and v' should tilt by $\sim 6^\circ$ latitude, while the results of Snyder et al. (1991) suggest that both should have even larger tilts. Even over the Pacific (not shown), where the 250-mb zonal wind exceeds 50 m s^{-1} , the poleward tilts of v'_g and v' in observed baroclinic waves do not exceed 3° and 7° latitude, respectively. Hence, the previous theoretical and modeling results appear to overestimate the observed poleward tilt with height of baroclinic waves. However, the details of jet structure or other factors could account for the

difference between the previous results and observations, so further investigation is required to explain this discrepancy.

Figure 1c shows that the structure of v'_a produces a poleward shift of v' at upper levels and an equatorward shift of v' at lower levels, enhancing the poleward tilt of v' . Thus, v'_a is important for the poleward tilt with height of v' in baroclinic waves, despite the fact that v'_a is smaller than v'_g by at least a factor of 5 (note the smaller contour interval in Fig. 1c). In the following sections, we investigate why v'_a has the structure that enhances the poleward tilt with height of v' in baroclinic waves.

4. Estimation of ageostrophic wind in baroclinic waves

An elegant explanation of the basic structure of the ageostrophic wind in baroclinic waves, with dominance of the zonal component at upper levels and dominance of the meridional component at lower levels, is given by Lim et al. (1991). We expand upon their analysis of the meridional ageostrophic wind, starting from the primitive equation zonal momentum equation:

$$\frac{Du}{Dt} - uv \frac{\tan(\phi)}{a} = f v - \frac{\partial \Phi}{\partial x} + F_{rx}, \quad (2)$$

where ϕ is latitude, a the radius of the earth, f the Coriolis parameter, Φ the geopotential, and F_{rx} the force due to friction in the zonal direction. Using $v'_g = f^{-1} \partial \Phi / \partial x$, the meridional ageostrophic wind can be written as

$$v_a \equiv v - v_g = f^{-1} \left[\frac{Du}{Dt} - uv \frac{\tan(\phi)}{a} - F_{rx} \right]. \quad (3)$$

Separating all variables into monthly means (denoted by overbars) and departures from monthly means (denoted by primes), and subtracting the monthly mean from (3), the departure of v_a from its monthly mean is

$$v'_a = f^{-1} \left\{ \frac{\partial u'}{\partial t} + \bar{\mathbf{v}}_3 \cdot \nabla_3 u' + \mathbf{v}'_3 \cdot \nabla_3 \bar{u} + \nabla_3 \cdot (\mathbf{v}'_3 u') - [\bar{u} v' + u' \bar{v} + (u' v)'] \frac{\tan(\phi)}{a} - F'_{rx} \right\}. \quad (4)$$

This is a complete primitive equation estimate for v'_a . Note that $(\mathbf{v}'_3 \cdot \nabla_3 u')' = \nabla_3 \cdot (\mathbf{v}'_3 u')$, and that $(\mathbf{v}'_3 u')' = \mathbf{v}'_3 u' - \nabla_3 u' \cdot \mathbf{v}'_3$ and $(u' v) = u' v' - u' \bar{v}$.

While friction cannot be directly estimated from the NCEP–NCAR reanalysis, all of the other terms in (4) can be retained and expanded to estimate v'_a as

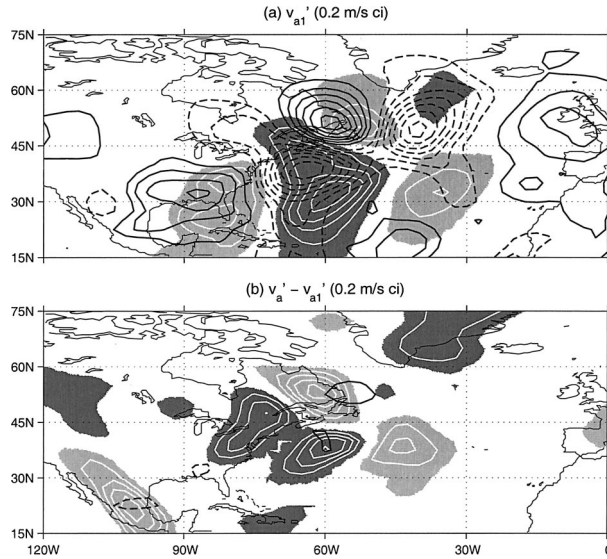


FIG. 2. (a) The full primitive equation estimate of the meridional ageostrophic wind v'_{a1} and (b) the difference between the observed meridional ageostrophic wind and this estimate $v'_a - v'_{a1}$, which at 925 mb is assumed to be due to the effect of friction. The contour/shading scheme for 250 and 925 mb is the same as in Fig. 1. The contour interval is 0.2 m s^{-1} .

$$v'_{a1} = f^{-1} \left\{ \left(\frac{\partial u'}{\partial t} + c \frac{\partial u'}{\partial x} \right) + (\bar{u} - c) \frac{\partial u'}{\partial x} + \bar{v} \frac{\partial u'}{\partial y} + \bar{\omega} \frac{\partial u'}{\partial p} + u' \frac{\partial \bar{u}}{\partial x} + v' \frac{\partial \bar{u}}{\partial y} + \omega' \frac{\partial \bar{u}}{\partial p} + \frac{\partial (u'^2)'}{\partial x} + \frac{\partial (v'u')'}{\partial y} + \frac{\partial (\omega'u')'}{\partial p} - [\bar{u}v' + u'\bar{v} + 2(u'v')'] \frac{\tan(\phi)}{a} \right\}, \quad (5)$$

where c is the zonal phase speed of the baroclinic wave. Phase speed c is estimated to be 12 m s^{-1} in the Atlantic storm track, based on the distance that v' maxima move between day -1 and day $+1$ in the regression analysis. Note that, when calculating the regression of a variance or covariance term such as $(u'v')'$, the product $u'v'$ is regressed on the reference time series, rather than regressing u' and v' separately and taking their product. In (5), the time tendency term is separated into two parts: $-c\partial u'/\partial x$, the part associated with a steady wave propagating zonally with phase speed c , and $\partial u'/\partial t + c\partial u'/\partial x$, the remainder due to growth or decay and nonzonal propagation. The former time tendency term is combined with the advection by the mean zonal wind to obtain the term $(\bar{u} - c)\partial u'/\partial x$, which represents advection by the mean zonal wind relative to the phase speed of the wave. Shown in Fig. 2a is the estimate of v'_a derived from (5), v'_{a1} , at 250 mb (black contours) and 925 mb (shaded with white contours). Comparing this to Fig. 1c, v'_{a1} and v'_a are very similar in structure, al-

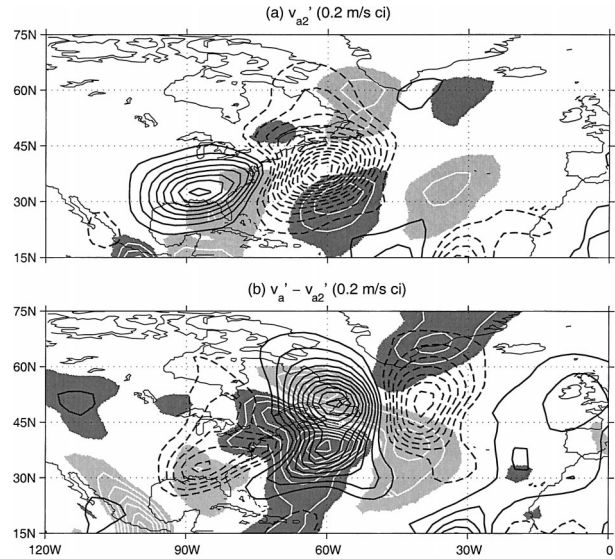


FIG. 3. As in Fig. 2, but for (a) the Lim et al. (1991) estimate of the meridional ageostrophic wind v'_{a2} and (b) the difference between the observed meridional ageostrophic wind and this estimate $v'_a - v'_{a2}$.

though the magnitude of v'_{a1} is too small at 925 mb. This is further illustrated by the difference $v'_a - v'_{a1}$ shown in Fig. 2b, which only has large values at 925 mb; in fact, at no level above 850 mb does $v'_a - v'_{a1}$ exceed 0.35 m s^{-1} . Since friction should be important only at lower levels, all terms other than friction appear to be accurately captured by (5), and we define $v'_{a\text{fric}} = v'_a - v'_{a1}$ at 850 mb and below as the part of v'_a due to the effects of friction.

Lim et al. (1991) arrive at a much simpler estimate of v'_a in a baroclinic wave:

$$v'_{a2} \approx f^{-1} \left[(\bar{u} - c) \frac{\partial u'_g}{\partial x} + v'_g \frac{\partial \bar{u}}{\partial y} \right], \quad (6)$$

where they neglect friction, assume a steady wave propagating zonally with phase speed c to ignore the $\partial u'/\partial t + c\partial u'/\partial x$ term, use plausible scaling arguments to keep just the two largest terms in (5), and retain only the geostrophic parts of u' and v' in the baroclinic wave. Figure 3a shows the estimate of v'_a derived from (6), v'_{a2} at 250 mb and 925 mb. Comparing this to Fig. 1c, v'_{a2} is quite different in structure from the actual v'_a . At 250 mb, v'_{a2} tends to oppose v' , while v'_a acts to shift v' poleward relative to v'_g ; at 925 mb, v'_{a2} is similar in structure to v'_a but is even weaker than v'_{a1} . The deficiencies at both levels mean that v'_{a2} indicates a smaller effect of the ageostrophic wind on the poleward tilt of v' than the actual v'_a . The difference $v'_a - v'_{a2}$ shown in Fig. 2b is as large as v'_a itself at both 250 and 925 mb.

Further analysis shows that some important terms have been left out of (6). Table 1 contains the maximum amplitude of each term in (5) between 20° and 70°N at the 250- and 925-mb levels; $f^{-1}(\bar{u} - c)\partial u'/\partial x$ and $f^{-1}v'\partial \bar{u}/\partial y$ have each been divided into their geostrophic

TABLE 1. Maximum amplitude (between 20° and 70°N) at 250 and 925 mb of each term in the estimate of v'_a derived from (5), v'_{a1} , as well as the residual $v'_a - v'_{a1}$ defined as v'_{afric} . Sets of terms enclosed in square brackets are components of the unbracketed terms immediately above them.

Term	250 mb	925 mb
$f^{-1}(\partial u'/\partial t + c\partial u'/\partial x)$	0.38	0.50
$f^{-1}(\bar{u} - c)\partial u'/\partial x$	2.07	0.57
$[f^{-1}(\bar{u} - c)\partial u'_g/\partial x]$	[3.23]	[0.49]
$[f^{-1}(\bar{u} - c)\partial u'_a/\partial x]$	[2.02]	[0.23]
$f^{-1}\bar{v}\partial u'/\partial y$	1.00	0.16
$f^{-1}\bar{\omega}\partial u'/\partial p$	0.06	0.07
$f^{-1}u'\partial \bar{u}/\partial x$	0.53	0.14
$f^{-1}v'\partial \bar{u}/\partial y$	2.08	0.51
$[f^{-1}v'_g\partial \bar{u}/\partial y]$	[2.04]	[0.36]
$[f^{-1}v'_a\partial \bar{u}/\partial y]$	[0.33]	[0.19]
$f^{-1}\omega'\partial u/\partial p$	0.24	0.49
$f^{-1}\nabla_3 \cdot (\mathbf{v}'_3 u')'$	1.70	0.52
$[f^{-1}\partial(v'u'^2)/\partial x]$	[1.67]	[0.62]
$[f^{-1}\partial(v'u')'/\partial y]$	[1.25]	[0.27]
$[f^{-1}\partial(\omega'u')'/\partial p]$	[0.40]	[0.22]
$f^{-1}\bar{u}\bar{v}\tan(\phi)/a$	0.79	0.11
$f^{-1}u'\bar{v}\tan(\phi)/a$	0.18	0.02
$f^{-1}2u'v'\tan(\phi)/a$	0.31	0.06
v'_{afric}	0.33	1.14

and ageostrophic components. While $f^{-1}(\bar{u} - c)\partial u'_g/\partial x$ and $f^{-1}v'_g\partial \bar{u}/\partial y$ are the two largest terms at 250 mb, $f^{-1}(\bar{u} - c)\partial u'_a/\partial x$ and the eddy momentum flux convergence $f^{-1}\nabla_3 \cdot (\mathbf{v}'_3 u')'$ are of comparable magnitude, and there are several other terms that are larger than v'_{afric} , the error of v'_{a1} . At 925 mb, it is clear that the two terms in (6) are merely among the largest terms in (5), and in fact the term attributed to friction, v'_{afric} , is the largest term. Thus, it is not surprising that v'_{a2} is a poor estimate of v'_a at both upper and lower levels. Kwon and Lim (1999) improve upon the estimate of Lim et al. (1991) by including the time tendency due to the growth rate of the baroclinic wave, which may be captured by the $f^{-1}(\partial u'/\partial t + c\partial u'/\partial x)$ term. While this term is important at 925 mb, there are a number of other terms that are larger at both 250 and 925 mb, so getting the time tendency right is an inadequate fix to the estimate of Lim et al. (1991). In fact, only two terms in (5) have an impact of less than 0.2 m s⁻¹ on v'_a at 250 mb, so nearly all must be included to adequately represent v'_a . While (5) cannot be regarded as an explanation for the structure of v'_a in baroclinic waves, because knowledge of the ageostrophic wind is needed to calculate most of the terms in (5), this is an important diagnostic result indicating that v'_a cannot be adequately estimated from geostrophic quantities alone.

5. Terms that enhance the poleward tilt of v'

There are three terms that noticeably enhance the poleward tilt of v' : the mean zonal wind advection term $f^{-1}(\bar{u} - c)\partial u'/\partial x$, the eddy momentum flux term $f^{-1}\nabla_3 \cdot (\mathbf{v}'_3 u')'$, and the residual attributed to friction v'_{afric} . Among the other terms in (5), $f^{-1}v'\partial \bar{u}/\partial y$ is the

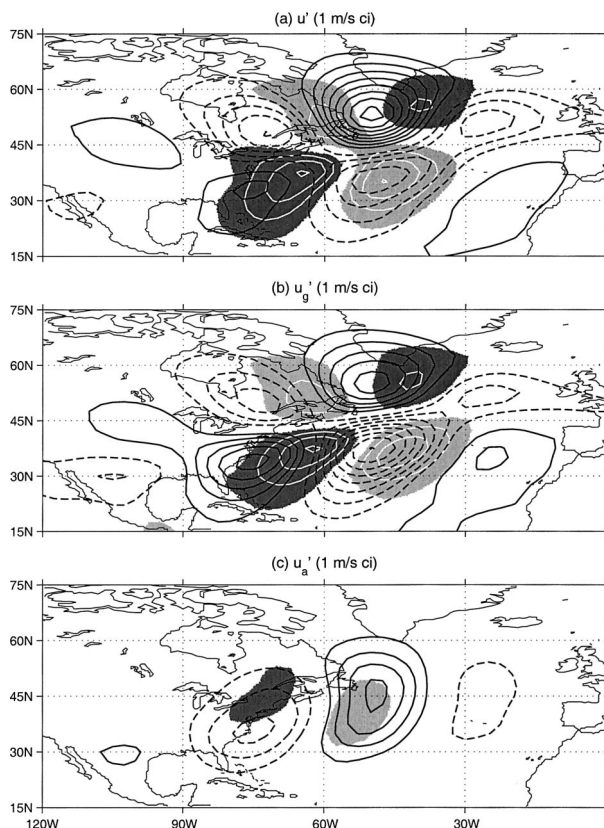


FIG. 4. As in Fig. 1, but for regressions of (a) total zonal wind u' , (b) geostrophic zonal wind u'_g , and (c) ageostrophic zonal wind u'_a . Note that the contour interval is 1 m s⁻¹ in all panels.

largest, but it shifts v' equatorward at both upper and lower levels, so it does not have much effect on the poleward tilt of v' . Terms $f^{-1}\bar{v}\partial u'/\partial y$ and $f^{-1}\bar{u}\bar{v}\tan(\phi)/a$ are large at upper levels, as $f^{-1}(\partial u'/\partial t + c\partial u'/\partial x)$ and $f^{-1}\omega'\partial u/\partial p$ are at lower levels, but all four have maxima centered on the storm track axis, so they also have little effect on the poleward tilt of v' . We now take a closer look at the three terms that do enhance the poleward tilt.

In order to understand the structure of the mean zonal wind advection term, $f^{-1}(\bar{u} - c)\partial u'/\partial x$, and the components of this term due to advection of u'_g and u'_a , we first examine the structure of u' , u'_g , and u'_a , which are shown in Fig. 4 at 250 mb (black contours) and 925 mb (shaded with white contours). Since u'_a is comparable in magnitude (4 m s⁻¹) to u'_g (8 m s⁻¹) at 250 mb, it is clear that u'_g is a poor estimate of u' , and it is not surprising that $f^{-1}(\bar{u} - c)\partial u'_a/\partial x$ is an important term in v'_{a1} . Figure 5 shows the terms $f^{-1}(\bar{u} - c)\partial u'/\partial x$, $f^{-1}(\bar{u} - c)\partial u'_g/\partial x$, and $f^{-1}(\bar{u} - c)\partial u'_a/\partial x$, at 250 and 925 mb. While the u'_a term is comparable in magnitude to the u'_g term at 250 mb, the u'_a term reinforces v' at 250 mb and has almost no effect at 925 mb, so it contributes very little to the poleward tilt of v' . The u'_g term, on the other hand, shifts the v' center poleward at 250 mb

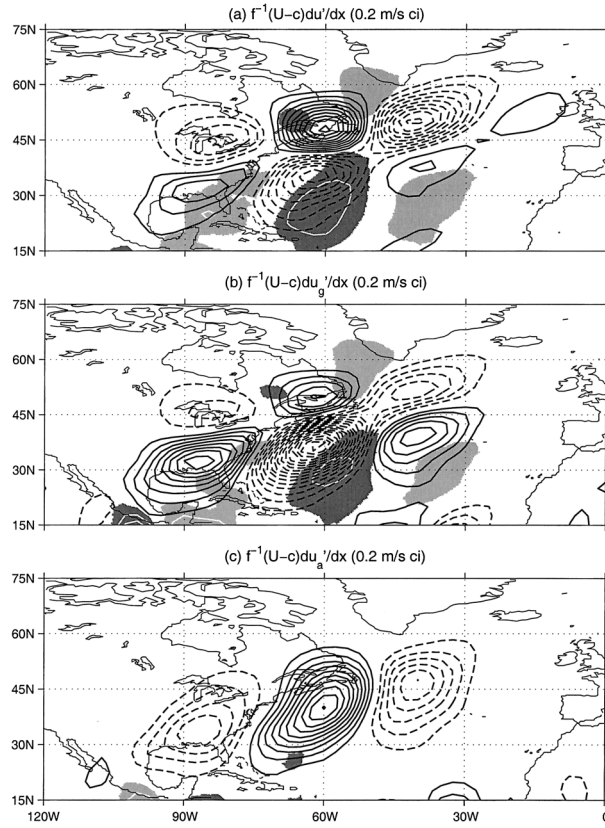


FIG. 5. Calculations of the following terms from the full estimate of the meridional ageostrophic wind v'_{a1} : (a) $f^{-1}(\bar{u} - c)\partial u'/\partial x$, the term due to advection of total zonal wind u' by the mean zonal wind; (b) $f^{-1}(\bar{u} - c)\partial u'_g/\partial x$, the term due to advection of the geostrophic zonal wind u'_g by the mean zonal wind; (c) $f^{-1}(\bar{u} - c)\partial u'_g/\partial x$, the term due to advection of the ageostrophic zonal wind u'_g by the mean zonal wind. The contour/shading scheme for 250 and 925 mb is the same as in Fig. 1. The contour interval is 0.2 m s^{-1} .

and equatorward at 925 mb, so most of the poleward tilt due to the $f^{-1}(\bar{u} - c)\partial u'/\partial x$ term is produced by the u'_g term, despite the comparable magnitude of the u'_a term. It is the change of sign of $(\bar{u} - c)$ from lower levels (negative) to upper levels (positive), coupled with the change of sign of u'_g from the equatorward flank to the poleward flank of the baroclinic wave packet, that allows this term to enhance the poleward tilt of v' . Since the SG equations include the full (geostrophic plus ageostrophic) advection of geostrophic momentum, the poleward tilt of v' that is due to the $f^{-1}(\bar{u} - c)\partial u'_g/\partial x$ term should be captured by both SG and PE models.

Figure 6a shows the eddy momentum flux term $f^{-1}\nabla_3 \cdot (\mathbf{v}'_3 u')$ at 250 and 925 mb. The largest influence of this term is a poleward shift of v' at upper levels; its magnitude is small at lower levels. The eddy momentum flux term is dominated by the zonal component $f^{-1}\partial(u'^2)/\partial x$, which is shown in Fig. 6b. The pattern of $f^{-1}\partial(u'^2)/\partial x$ at 250 mb is due to a maximum in $(u'^2)'$ centered near the southern tip of Greenland, which is related to the large center of positive u' shown in Fig.

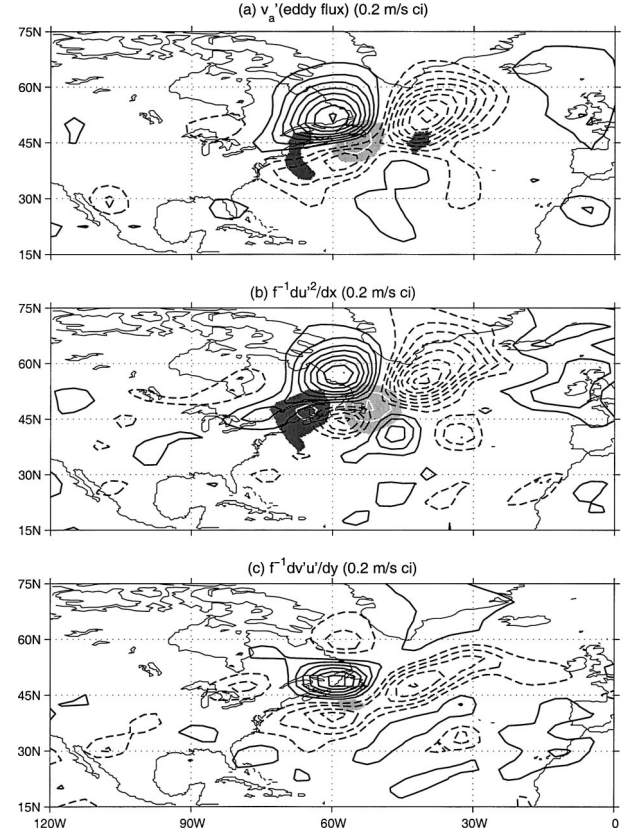


FIG. 6. As in Fig. 5, but for the following terms from the estimate v'_{a1} : (a) $f^{-1}\nabla_3 \cdot (\mathbf{v}'_3 u')$, the term due to eddy momentum flux convergence; (b) $f^{-1}\partial(u'^2)/\partial x$, the term due to the zonal component of eddy momentum flux convergence; (c) $f^{-1}\partial(v'u')/\partial y$, the term due to the meridional component of eddy momentum flux convergence.

4a. This positive u' center is larger than the corresponding u'_g center due to enhancement by u'_a (see Figs. 4b and 4c), so the eddy momentum flux term owes much of its structure to the large magnitude of u'_a . The meridional component of the eddy momentum flux term, shown in Fig. 6c, also contributes to the poleward tilt of v' , but it is less important than the zonal component, and the vertical component (not shown) has little effect on the poleward tilt. As shown by Snyder et al. (1991), the advection of ageostrophic vorticity is important in increasing the poleward tilt of baroclinic waves in PE models relative to SG models, so, due to the importance of u'_a in the eddy momentum flux term, we expect that this term will be underestimated in SG models relative to PE models.

The structure of the residual attributed to friction v'_{afric} is shown in Fig. 2b. Ignoring the centers of v'_{afric} near Mexico, the eastern United States, and Greenland, which are probably affected by topography, the centers of v'_{afric} line up nicely with the centers of 925-mb u' shown in Fig. 4a. The residual friction term v'_{afric} is also of the same sign as u' , or of the opposite sign as the force due to friction, which is consistent with the sign

of the friction term $-f^{-1}F_{rx}$ from (4). Since v'_{afric} is shifted somewhat to the west compared to v'_g at 925 mb (see Fig. 1b), v'_{afric} not only shifts v' equatorward but also contributes to its SW–NE tilt at 925 mb. Because friction is not included in the previous SG and PE modeling studies, we expect the friction term to enhance the poleward tilt of observed baroclinic waves relative to those found in SG and PE models, so it is surprising that these models appear to overestimate the poleward tilt relative to observed baroclinic waves.

When the sum of the three terms $f^{-1}(\bar{u} - c)\partial u'_g/\partial x$, $f^{-1}\nabla_3 \cdot (\mathbf{v}'_3 u')'$, and v'_{afric} is added to v'_g (not shown), the resulting poleward tilt is approximately the same as that of the observed v' , so these three terms do indeed capture the full poleward tilt of v' .

6. Conclusions

Regression analysis of NCEP–NCAR reanalysis data shows that observed baroclinic waves do indeed tilt poleward with height, as predicted by theoretical and modeling studies of nongeostrophic effects in baroclinic waves (e.g., Hoskins 1975; Snyder et al. 1991) and suggested by figures from regression analyses of baroclinic wave structure in GCM simulations (Chang 2001). However, the observed tilt is smaller than predicted by these previous studies. We have shown that the meridional ageostrophic wind v'_a acts to enhance the poleward tilt of v' over the tilt it would have if it were purely geostrophic, even though v'_a is smaller than v' by a factor of 5.

We have also extended the work of Lim et al. (1991) and Kwon and Lim (1999) to obtain a more accurate estimate of the structure of v'_a in baroclinic waves based on the need to maintain force balance and keep the baroclinic wave intact as a propagating entity. An analysis of the terms in this new estimate indicates that nearly all must be retained to produce a good estimate of v'_a , and that v'_a cannot be adequately estimated from geostrophic quantities alone. We show that three terms act in the same sense to produce nearly all of the poleward tilt of v' in the observed baroclinic waves: 1) the advection of geostrophic u' by the mean zonal wind, 2) the convergence of the eddy momentum flux, and 3) the effect of friction. While the first term is captured by both SG and PE models, term 2 is likely to be underestimated by SG models because of the importance of the ageostrophic zonal wind u'_a in the eddy momentum flux term, and term 3 is not included in any of the SG and PE studies mentioned in the introduction. Thus, it is surprising that the SG and PE models overestimate the poleward tilt with height of v' in observed baroclinic waves; this discrepancy is left to future work.

Although it has been known for some time that baroclinic waves tilt poleward with height, we are unaware of any observational study of this poleward tilt. The poleward tilt of baroclinic waves is more than just an academic curiosity, since it explains the well-known obser-

vation that the upper-level storm tracks tend to occur poleward of near-surface baroclinic regions under the jets (e.g., Blackmon et al. 1977). In addition, the poleward tilt with height of v' in baroclinic waves may play a role in the suppression of the Pacific storm track in midwinter, when the strong PV gradients in the Pacific subtropical jet shift equatorward of the near-surface baroclinic zone (Yin 2002). The seasonal variation of the ageostrophic wind structure in baroclinic waves over the Pacific, where the terms in our estimate of v'_a undergo large changes in structure due to the strengthening of the subtropical jet, also remains a subject for future work.

Acknowledgments. We would like to thank Mike Wallace for valuable comments on an earlier version of the manuscript, and Greg Hakim for sharing his experience in studying the structure of baroclinic waves. We also appreciate the insightful comments of Chris Snyder and two anonymous reviewers, which motivated us to do additional calculations and sharpened the presentation of this work. This publication is funded by the Joint Institute for the Study of the Atmosphere and Ocean (JISAO) under NOAA Cooperative Agreement NA17RJ11232, and was completed while the first author held a postdoctoral fellowship from the NOAA Climate and Global Change Program.

REFERENCES

- Blackmon, M. L., J. M. Wallace, N.-C. Lau, and S. L. Mullen, 1977: An observational study of the Northern Hemisphere wintertime circulation. *J. Atmos. Sci.*, **34**, 1040–1053.
- , Y.-H. Lee, and J. M. Wallace, 1984: Horizontal structure of 500 mb height fluctuations with long, intermediate, and short time scales. *J. Atmos. Sci.*, **41**, 961–979.
- Chang, E. K. M., 1993: Downstream development of baroclinic waves as inferred from regression analysis. *J. Atmos. Sci.*, **50**, 2038–2053.
- , 2001: GCM and observational diagnoses of the seasonal and interannual variations of the Pacific storm track during the cool season. *J. Atmos. Sci.*, **58**, 1784–1800.
- Derome, J., and C. L. Dolph, 1970: Three-dimensional non-geostrophic disturbances in a baroclinic zonal flow. *Geophys. Fluid Dyn.*, **1**, 91–122.
- Eady, E. T., 1949: Long waves and cyclone waves. *Tellus*, **1**, 35–52.
- Hoskins, B. J., 1975: The geostrophic momentum approximation and the semigeostrophic equations. *J. Atmos. Sci.*, **32**, 233–242.
- Kwon, H. J., and G.-H. Lim, 1999: Reexamination of the structure of the ageostrophic wind in baroclinic waves. *J. Atmos. Sci.*, **56**, 2512–2521.
- Lim, G. H., and J. M. Wallace, 1991: Structure and evolution of baroclinic waves as inferred from regression analysis. *J. Atmos. Sci.*, **48**, 1718–1732.
- , J. R. Holton, and J. M. Wallace, 1991: The structure of the ageostrophic wind field in baroclinic waves. *J. Atmos. Sci.*, **48**, 1733–1745.
- McIntyre, M. E., 1965: A separable nongeostrophic baroclinic stability problem. *J. Atmos. Sci.*, **22**, 730–731.
- Snyder, C., W. C. Skamarock, and R. Rotunno, 1991: A comparison of primitive-equation and semigeostrophic simulations of baroclinic waves. *J. Atmos. Sci.*, **48**, 2179–2194.
- Yin, J. H., 2002: The peculiar behavior of baroclinic waves during the midwinter suppression of the Pacific storm track. Ph.D. thesis, University of Washington, 121 pp.